

## Old Dominion University ODU Digital Commons

---

Civil & Environmental Engineering Faculty  
Publications

Civil & Environmental Engineering

---

2003


# Anisotropy and Its Relation to Liquefaction Resistance of Granular Material

Isao Ishibashi

*Old Dominion University*, [iishibas@odu.edu](mailto:iishibas@odu.edu)

Omer F. Capar

Follow this and additional works at: [https://digitalcommons.odu.edu/cee\\_fac\\_pubs](https://digitalcommons.odu.edu/cee_fac_pubs)

 Part of the [Geology Commons](#), [Geotechnical Engineering Commons](#), and the [Soil Science Commons](#)

---

### Repository Citation

Ishibashi, Isao and Capar, Omer F., "Anisotropy and Its Relation to Liquefaction Resistance of Granular Material" (2003). *Civil & Environmental Engineering Faculty Publications*. 28.  
[https://digitalcommons.odu.edu/cee\\_fac\\_pubs/28](https://digitalcommons.odu.edu/cee_fac_pubs/28)

### Original Publication Citation

Ishibashi, I., & Capar, O. F. (2003). Anisotropy and its relation to liquefaction resistance of granular material. *Soils and Foundations*, 43(5), 149-159. doi:10.3208/sandf.43.5\_149

This Article is brought to you for free and open access by the Civil & Environmental Engineering at ODU Digital Commons. It has been accepted for inclusion in Civil & Environmental Engineering Faculty Publications by an authorized administrator of ODU Digital Commons. For more information, please contact [digitalcommons@odu.edu](mailto:digitalcommons@odu.edu).

## ANISOTROPY AND ITS RELATION TO LIQUEFACTION RESISTANCE OF GRANULAR MATERIAL

ISAO ISHIBASHI<sup>1)</sup> and OMER F. CAPAR<sup>2)</sup>

### ABSTRACT

This research establishes quantitative relationships between soil's anisotropy and liquefaction resistance for granular materials. Uniform medium density ( $D_r = 50\%$ ) sand specimens were prepared using three different sample preparation techniques (air pluviated (AP), moist tamped (MT), and moist vibrated (MV)) to create different initial soil fabrics. Undrained cyclic triaxial tests were then performed to determine the liquefaction resistance of each soil specimen. On the same specimens in the triaxial cell, vertical and horizontal compression wave velocities and vertical shear wave velocity ( $V_s$ ) were measured using piezoelectric bender elements. Anisotropic (transversely isotropic) elastic constants of the soil specimens were determined from the elastic wave measurements and additional consolidation test data. With the aid of additional data from earlier discrete element model (DEM) simulations, anisotropic parameters, which influence the liquefaction resistance, were examined. It was found that when liquefaction resistance is divided by  $G_{12}/(E_1/E_2)^3$ , by  $G_{\text{average}}/(E_1/E_2)^3$ , or by  $V_s^{5.0}$ , liquefaction resistance curves converge to a unique curve regardless of the sample preparation techniques. Liquefaction Stress Ratio Reduction Factor (LSRRF) was introduced to estimate the reduction of liquefaction cyclic stress ratio of an anisotropic specimen from the isotropic specimen as simple functions of  $(E_1/E_2)^{-5.0}$  or  $(V_s/V_{s(\text{iso.})})^{5.0}$ .

**Key words:** anisotropy, discrete element model, elastic modulus, granular material, laboratory test, liquefaction, numerical simulation, piezoelectric sensor, wave velocity (IGC: D7)

### INTRODUCTION

The 1964 Niigata and Alaska earthquakes have led many researchers to study the liquefaction problems over the past 30 years. The evaluation of liquefaction resistance of saturated sand deposits has included laboratory and in-situ testing techniques. In the laboratory studies, cyclic triaxial test, cyclic simple shear test, etc., have been conducted to investigate the effects of soil density, gradation, cyclic stress amplitude, and other parameters controlling liquefaction resistance. Since obtaining high-quality undisturbed sand and gravel specimens requires extremely difficult and expensive procedures such as in-situ freezing methods (Yoshimi et al., 1984, 1989), in most cases, soil specimens had to be reconstituted in the laboratory at the estimated in-situ density of soil. However, laboratory reconstituted specimens and undisturbed specimens exhibited quite different liquefaction resistances. Furthermore, researchers (Ladd, 1974; Mulilis et al., 1977; Toki et al., 1986; Tatsuoka et al., 1986) experimentally showed that the liquefaction resistance is highly influenced by different sample preparation techniques. It is believed that those differences are due to soil fabric or inherent anisotropy

created by different sample preparation techniques.

Arulmoli et al. (1985) correlated liquefaction resistance to soil's anisotropy based on electrical resistance measurements in vertical and horizontal directions. They showed that the anisotropic index  $A$  had a strong influence on liquefaction resistance and the proposed electric index is strongly related to an elastic material property (the maximum shear modulus  $G_{\text{max}}$  at a very low strain amplitudes). De Alba et al. (1984) noticed experimentally that elastic waves are also affected by anisotropy of soils. Ishibashi and Agarwal (1991) and Agarwal and Ishibashi (1992) measured  $P$ -wave and  $S$ -wave velocities along several directions relative to the principal stress axes in the cubical granular specimens. Their work suggested that elastic properties, in particular, the directional wave velocity measurements could identify the anisotropy of the granular materials. In addition, Ishibashi and Kiku (1995) presented discrete element model simulations to relate the effect of initial anisotropy by means of directional elastic moduli to liquefaction resistance. The works of Tokimatsu et al. (1986), Tokimatsu and Uchida (1990), and Andrus and Stokoe (2000) proposed promising empirical correlations between liquefaction resistance of sand deposits and

<sup>1)</sup> Professor, Department of Civil and Environmental Engineering, Old Dominion University, Norfolk, Virginia 23529 (iishibas@odu.edu).

<sup>2)</sup> Assistant Professor, Zonguldak Karaelmas University, Department of Civil Engineering, Zonguldak, 67100, formerly Doctoral Student, Old Dominion University.

Manuscript was received for review on July 29, 2002.

Written discussions on this paper should be submitted before May 1, 2004 to the Japanese Geotechnical Society, Sugayama Bldg. 4F, Kanda Awaji-cho 2-23, Chiyoda-ku, Tokyo 101-0063, Japan. Upon request the closing date may be extended one month.

shear wave velocities measured in the field. However, these efforts were based solely on field empirical correlations without clear knowledge of the anisotropic soil behavior and its relation to wave velocities.

In the research reported herein, laboratory experiments have been conducted to describe anisotropy and to evaluate liquefaction resistance under cyclic loading for a sandy soil. Three different sample preparation techniques were utilized to obtain different initial soil fabrics. By measuring  $P$ -wave and  $S$ -wave velocities in the vertical direction and  $P$ -wave velocity in the horizontal direction through triaxial specimens, the anisotropy of the specimens was quantified. Cyclic triaxial tests were then conducted to determine liquefaction resistance for each soil sample. The relationship between anisotropy and liquefaction resistance is quantitatively established based on those experimental results. In addition, discrete element numerical simulation results (Ishibashi and Kiku, 1995) are utilized to supplement the laboratory data on liquefaction and anisotropic elastic constants. In the following section, the laboratory experimental procedures are summarized. The detailed descriptions of the experiments can be seen in Capar (2000).

In the following discussions, earlier DEM simulations (Ishibashi and Kiku, 1995) used the isotropic effective confining stress of 138 kPa for their elastic moduli computation and liquefaction simulations. The current laboratory wave measurements, liquefaction, consolidation tests and numerical recovery of elastic moduli use data under 68.9 kPa isotropic effective confining stress. The analyses, however, are all based on various ratios, so that the difference on the effective confining stresses and different soil types (real soil vs. spheres) do not hinder further discussions.

## EXPERIMENTS AND DISCRETE ELEMENT MODEL (DEM) SIMULATIONS

### *Cyclic Triaxial Device*

A standard triaxial cell with a 71 mm specimen diameter was modified for this research. Monotonic and cyclic axial loads were introduced independently by two different pneumatic loaders from the top and from the base of the cell, respectively. The lateral pressure was kept constant during the cyclic loading; thus, the cyclic stress ratio (CSR) for liquefaction was defined as  $(\sigma_{\text{cyclic}}/2\sigma'_0)$ , where  $\sigma_{\text{cyclic}}$  is the cyclic deviator stress and  $\sigma'_0$  is the initial effective mean stress.

### *Consolidation Test*

In the same triaxial test setup, a series of isotropic consolidation tests were conducted in order to determine volumetric characteristics of the specimens. Specimens were first saturated under 68.9 kPa confining pressure and 34.5 kPa back pressure with  $\text{CO}_2$  gas and then deaired water circulations. Saturation process was checked by pulse transmission technique.  $P$ -wave arrival time in vertical direction was monitored. When the saturation degree was increased, it transmitted faster and higher

amplitude  $P$ -waves. When the velocity of saturated specimens was reached, it was assumed that the specimens were nearly fully saturated for the purpose of volumetric strain measurement by means of the amount of expelled water from the specimen during the consolidation process. Note that the pore pressure parameter  $B$ -value check (more than 0.94) was used to assure a satisfactory saturation prior to liquefaction tests. After specimens were saturated under 68.9 kPa confining and 34.5 kPa back pressure, isotropic consolidation stresses were increased step by step from 68.9, 138, 207, 276, and to 345 kPa. During each consolidation load step, volume change was measured in a bullet, which is connected to the specimen through the drainage line, after the water height in the bullet was stabilized. The axial strain was measured at a displacement transducer, which was connected to the vertical loading piston.

### *Wave Velocity Measurements with Piezoelectric Bender Elements*

Piezoelectric bender elements ( $10 \times 10 \times 0.6$  mm) were used to generate and to detect compression and shear waves in the specimen in triaxial device. Serial connected bender elements (Dyvik and Madshus, 1985; Thomann and Hryciw, 1990) were used for both generators and receivers for their simplicity of electric connections. Two bender elements are embedded in the top cap and the pedestal of the triaxial device as transmitters and receivers in the vertical direction for  $P$ - and  $S$ -waves. In addition, a pair of bender elements is placed at the outside of specimen membrane on opposing sides of the specimen as seen in Fig. 1. Each bender element is attached to one end of the cantilever arm and the other end is connected to a small rod, which is controlled from the outside of the triaxial cell through a sealed hole on the chamber. Pulling the rod gently pushes the bender element against the specimen by the cantilever mechanism.

Electrical signals were generated using a pulse/function generator. A single-frequency sinusoidal waveform was chosen as the input signal. The amplitude of generated wave signals was 10 volts. However, since sandy materials have large damping characteristics, the 10 volts of input signal were amplified to 160 volts by means of the power amplifier and further amplified through a transformer to step up the voltage up to 960 volts AC. Experimental trials showed that the best readings occurred with input signal frequencies between 17 to 22 kHz for vertical  $P$ -wave bender elements, between 20 to 30 kHz for horizontal  $P$ -waves, and between 5 to 10 kHz for  $S$ -waves.

Input and output signals produced by piezoelectric bender elements were recorded with a digital oscilloscope to calculate the travel time. Due to possible traveling time delays through electric cables and instruments, calibrations on the traveling time were made. For  $P$ -wave measurements, the transmitter and receiver were in direct contact and the time delay was measured. There was, indeed, 5  $\mu\text{sec}$  time delay between the input and the arrival signals in the setup and thus this delay time was subtracted in all

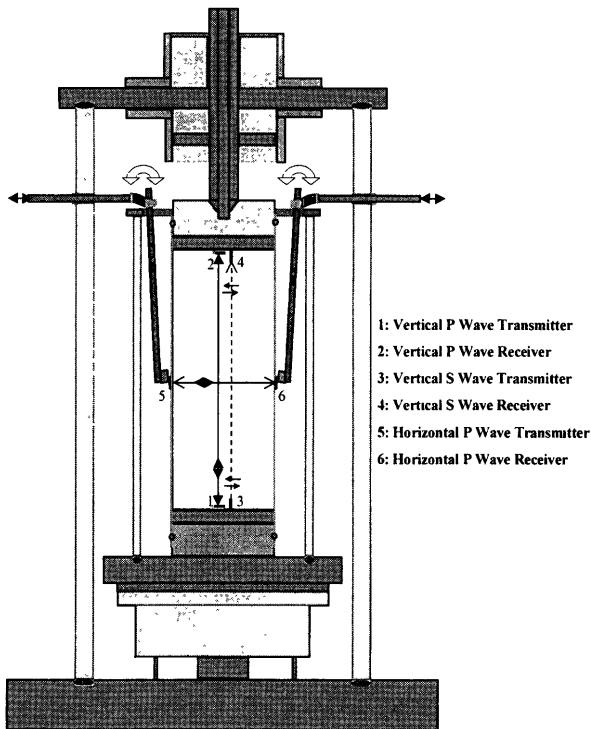


Fig. 1. Triaxial cell setup with bender elements

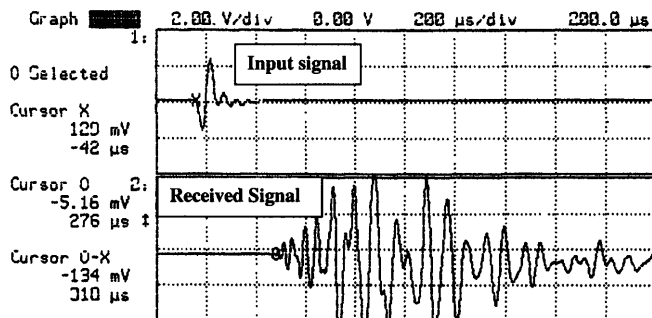


Fig. 2. Typical transmitted and received wave signals

*P*-wave measurements. For the vertical direction *S*-wave measurements, by placing the transmitter and receiver in several facing distances in the air, the first arrival times were measured. By extrapolating the result to the zero arrival time, the equivalent zero distance between the transmitter and receiver was established and thus this zero distance was used as the reference zero point to calculate traveling distances in all *S*-wave measurements. The 5  $\mu$ sec delay time correction was not applied in this case since the zero distance calibration includes the time delay effect if it exists. A sampling rate of  $200 \times 10^6$  samples per second provided sufficient resolution for this research. Typical transmitted and received signals are shown in Fig. 2.

#### Material Used for Cyclic Liquefaction and Wave Measurements

A uniformly graded sand (Virginia Beach Sand) was chosen for this testing program. The material contains

less than 0.74% fines. The sand is subangular with following indices: specific gravity,  $G_s = 2.685 \pm 0.012$ ; mean grain size,  $D_{50} = 0.29$  mm; coefficient of uniformity,  $C_u = 2.04$ ; coefficient of gradation,  $C_c = 0.91$ ; maximum void ratio;  $e_{\max} = 0.82$ ; and minimum void ratio,  $e_{\min} = 0.59$ . In this study, the soil was re-constituted to a nominal 50% relative density ( $D_r$ ). The actual range of relative densities was between 48% and 52%. The variation in the values of wave velocities ( $V_{pv}$ ,  $V_{sv}$  and  $V_{ph}$ ) under 34.5 kPa effective confining pressure were approximately  $\pm 2.1$ ,  $\pm 3.8$  and  $\pm 3.2\%$ , respectively, and under 68.9 kPa effective confining pressure were  $\pm 1.4$ ,  $\pm 3.1$  and  $\pm 3.3\%$ , respectively.

#### Sample Preparation Techniques

Triaxial specimens (approximately 71 mm diameter with 142 mm high) were prepared using the following three different techniques:

**Air Pluviation:** A known amount of air-dried Virginia Beach Sand was poured into a flask. The flask was closed with a rubber stopper that has a 6.4 mm diameter nozzle. The flask was placed upside-down above the mold, and by rotating the flask, sand was poured into the mold from a controlled height until all of the sand was dispersed. To obtain  $D_r \approx 50\%$ , proper nozzle size (6.4 mm diameter), height of the drop (152 mm), and rotation speed were established by trial and error.

**Moist Tamping:** The specimen was formed in five layers. The first layer thickness at the bottom was 48 mm in order to protect the piezoelectric transducers at the bottom from the tamping effects. The other layers were 25.4 mm thick. The desired weight of air-dried sand for each layer was poured into a pan and mixed with a certain amount of water to have a moisture content of 8%, which was found to be the most suitable for moist specimen preparation by trials and errors. After the creation of a homogeneous mixture of moist sand, the mixture was poured into the mold. The surface was leveled. The mixture was compacted by dropping a tamping rod (70 mm diameter) from a height of 25.4 mm until the desired layer thickness was achieved.

**Moist Vibration:** In order to have a uniform soil specimen and to apply a large amount of vibration energy, a soil specimen was formed in 10 layers. The first two layers were 24 mm each to protect the piezoelectric bender elements at the surface of the pedestal and all other layers were 12.7 mm. To prepare each layer, a beaker was filled with the desired weight of dry soil and a certain amount of water. They were mixed enough to have a homogeneous moist mixture with 8% water content. The mixture was poured into a split mold and the surface was leveled. A surcharge load of 7.7 kPa was placed on the layer. A modified hand vibrator was contacted firmly to the side of the mold until the desired height was achieved. The frequency of vibration was 1 kHz.

#### Discrete Element Model Simulations

To supplement laboratory data on liquefaction and elastic wave measurements, numerical simulations from

**Table 1. Material properties of DEM simulations (Ishibashi and Kiku, 1995)**

Glass beads material properties		
Shear modulus	2.0 × 10 <sup>8</sup> MPa	
Poisson's ratio	0.2	
Contact friction coefficient	0.35	
Glass beads assembly		
	Mixing ratio of two size beads	
Particle diameter (mm)	0.215	0.256
Number of particles	216	216
Weight ratio	1	1.688
Final porosity (Relative density)	0.380 (38.8%)	

**Table 2. Specimen preparations for DEM simulations (Ishibashi and Kiku, 1995)**

Specimens	Stage of porosity 0.967 → 0.473 → 0.380	Preshearing
<b>M1</b> (isotropic)	isotropic compression → $\Delta\epsilon_h = \Delta\epsilon_v$	none
<b>M2</b>	isotropic comp. →   anisotropic comp. → $\Delta\epsilon_h = \Delta\epsilon_v$   $\Delta\epsilon_h = 0$	none
<b>M3</b>	isotropic compression → $\Delta\epsilon_h = \Delta\epsilon_v$	$\gamma_{\max} = 0.3\%$ in $\theta = 0$ direction under $\sigma_1 + \sigma_2 + \sigma_3 = 413$ kPa
<b>M4</b>	isotropic compression → $\Delta\epsilon_h = \Delta\epsilon_v$	$\gamma_{\max} = 0.9\%$ in $\theta = 0$ direction under $\sigma_1 + \sigma_2 + \sigma_3 = 413$ kPa
<b>M5</b>	isotropic compression → $\Delta\epsilon_h = \Delta\epsilon_v$	6 cycles of $\Delta\epsilon_v = 0.0024\%$ under $\Delta\epsilon_h = 0$

the authors' earlier work (Ishibashi and Kiku, 1995) were incorporated into this research. The work is briefly summarized in this section. The authors used a three-dimensional discrete element model "TRUBAL" (Cundall, 1988) to numerically create different levels of anisotropic specimens. TRUBAL can simulate behavior of a sphere assembly under controlled cubic strain boundaries based on non-linear Hertzian normal contact and linear Mindlin shear contact laws. It monitors movements of spheres and contact forces and thus computes stress and strain of the assembly at its periodic boundaries. Boundary strains are inputs, but the boundary stresses can be also controlled with a servo-mechanism if needed. Due to its cubical shape and the use of periodical boundaries, this discrete element model may be best suited for various element tests of granular assembly. Loose glass beads assemblies, which consist of two different diameter spheres (Table 1), were numerically prepared and five different specimens were created as summarized in Table 2. The specimens were first randomly generated

and compacted isotropically under a non-gravitational field to a very loose state (porosity  $n = 0.967$ ). The M1 specimen was isotropically compressed by moving the three facing boundaries of the cubic specimen with a same strain rate until achieving the targeted initial porosity,  $n = 0.380$ . The M2 specimen was first compressed isotropically to  $n = 0.473$  and two horizontal plane boundaries were then moved closer to each other while four other vertical boundaries were kept unmoved until a porosity of  $n = 0.380$  was achieved. All other specimens (M3, M4, and M5) were isotropically compressed to the porosity (0.380) with the same method used for M1. The M3, M4, and M5 specimens were further presheared to create different levels of anisotropy as shown in Table 2. During the preshearing, the density of the original specimens was retained in the specimen. The M1 specimen is initially isotropic and the M2 through M5 specimens are expected to have different levels of anisotropy relative to their transversely isotropic axis. For those specimens, small incremental compressive strain ( $1.1$  to  $1.3 \times 10^{-4}$ ) were applied from various directions with angle  $\theta$  relative to the vertical while the normal strains perpendicular to the  $\theta$  direction were kept zero. Compression moduli  $E_\theta$  was then calculated as  $\Delta\sigma_\theta/\Delta\epsilon_\theta$ , in which  $\Delta\sigma_\theta$  is the induced compressive stress due to the applied incremental strain  $\Delta\epsilon_\theta$  in the  $\theta$  direction. Directional shear moduli  $G_\theta$  are also obtained similarly as  $\Delta\tau_\theta/\Delta\gamma_\theta$ , where  $\Delta\tau_\theta$  and  $\Delta\gamma_\theta$  are the shear stress and strain increments in the  $\theta$  direction, respectively. In the above simulations, TRUBAL can only move vertical and horizontal boundaries of its cubical specimen, and thus in order to compute  $\Delta\sigma_\theta$ ,  $\Delta\epsilon_\theta$ ,  $\Delta\tau_\theta$  and  $\Delta\gamma_\theta$  transformations of stress and strain increments from  $\Delta\sigma_1$ ,  $\Delta\epsilon_1$ ,  $\Delta\sigma_2$  and  $\Delta\epsilon_2$  are needed by using Mohr's stress and strain circles as:

$$\Delta\sigma_\theta = \frac{\Delta\sigma_1 - \Delta\sigma_2}{2} \left(1 + \frac{1}{\cos 2\theta}\right) + \Delta\sigma_2 \quad \text{for } \theta \neq 45^\circ,$$

$$\text{or } \Delta\sigma_\theta = -\Delta\tau_{12} + \Delta\sigma_2 \quad \text{for } \theta = 45^\circ \quad (1)$$

$$\Delta\epsilon_\theta = -\frac{\Delta\gamma_{12}}{\sin 2\theta} \quad \text{for } \theta \neq 0^\circ, 90^\circ,$$

$$\text{or } \Delta\epsilon_\theta = \Delta\epsilon_1 \quad \text{for } \theta = 0^\circ,$$

$$\text{or } \Delta\epsilon_\theta = \Delta\epsilon_2 \quad \text{for } \theta = 90^\circ \quad (2)$$

$$\Delta\tau_\theta = \frac{\Delta\tau_{12}}{\cos 2\theta} \quad \text{for } \theta \neq 45^\circ,$$

$$\text{or } \Delta\tau_\theta = \frac{\Delta\sigma_1 - \Delta\sigma_2}{2} \quad \text{for } \theta = 45^\circ \quad (3)$$

$$\Delta\gamma_\theta = \frac{\Delta\gamma_{12}}{\cos 2\theta} \quad \text{for } \theta \neq 45^\circ,$$

$$\text{or } \Delta\gamma_\theta = 2\Delta\epsilon_1 \quad \text{for } \theta = 45^\circ \quad (4)$$

Another note in TRUBAL simulation is that  $E_\theta$  and  $G_\theta$  are calculated for the plain strain condition (i.e. the normal strains perpendicular to the  $\theta$  direction were kept zero) due to a convenience of TRUBAL application (strain controlled boundary). This simulation would give us clear indication of directional variation of those elastic moduli. Those values, however, may slightly differ from

the moduli defined in Eq. (5) in the proceeding discussion, which can be obtained from the plan strain condition.

In the numerical simulations, cyclic simple shear tests under a constant volume were also performed to obtain equivalent pore water buildup in dry specimens (Finn et al., 1978). That is, cyclic uniform shear strains in the horizontal-vertical plane were applied to the specimens while keeping the vertical and lateral normal stresses constant. Under such conditions, measured changes in the vertical normal stress are equivalent to the changes in the pore pressure in saturated specimens.  $(\sigma_{v0} - \sigma_v) / \sigma_{v0}$  is defined as the equivalent pore water pressure ratio, where  $\sigma_{v0}$  is the initial vertical normal stress and  $\sigma_v$  is the

changed vertical normal stress. The simulation results are presented and discussed later in the paper.

**COMPUTATION OF TRANSVERSELY ISOTROPIC ELASTIC CONSTANTS**

Cylindrical triaxial specimens and level ground field soils are reasonably assumed to be transversely isotropic. We take the symmetrical axis 1 in the vertical direction and take axes 2 and 3 in the horizontal directions; thus, the plane 2-3 becomes a plane of symmetry. For such transversely isotropic materials, the elastic stress-strain relation can be written as:

$$\begin{bmatrix} \varepsilon_1 \\ \varepsilon_2 \\ \varepsilon_3 \\ \gamma_{12} \\ \gamma_{13} \\ \gamma_{23} \end{bmatrix} = \begin{bmatrix} 1/E_1 & -\nu_{21}/E_2 & -\nu_{21}/E_2 & 0 & 0 & 0 \\ -\nu_{12}/E_1 & 1/E_2 & -\nu_{32}/E_2 & 0 & 0 & 0 \\ -\nu_{12}/E_1 & -\nu_{23}/E_2 & 1/E_2 & 0 & 0 & 0 \\ 0 & 0 & 0 & 1/G_{12} & 0 & 0 \\ 0 & 0 & 0 & 0 & 1/G_{12} & 0 \\ 0 & 0 & 0 & 0 & 0 & 1/G_{23} \end{bmatrix} \begin{bmatrix} \sigma_1 \\ \sigma_2 \\ \sigma_3 \\ \tau_{12} \\ \tau_{13} \\ \tau_{23} \end{bmatrix} \tag{5}$$

There are, in general, eight constants in the relations ( $E_1, E_2, G_{12}, G_{23}, \nu_{12}, \nu_{21}, \nu_{23},$  and  $\nu_{32}$ ). However, in the elastic theory, there are three well established relationships;

$$\frac{\nu_{12}}{E_1} = \frac{\nu_{21}}{E_2} \tag{6}$$

$$\nu_{32} = \nu_{23} \tag{7}$$

$$\text{and } G_{23} = \frac{E_2}{2(1 + \nu_{23})} \tag{8}$$

Therefore, five unique constants remain in Eq. (5). From elastic wave theory, the  $P$ -wave velocity in the vertical direction is:

$$V_{pv} = \sqrt{\frac{C_{11}}{\rho}}, \text{ where } C_{11} = \frac{E_1 E_2 (-1 + \nu_{32})}{-E_2 + 2E_1 \nu_{21}^2 + E_2 \nu_{32}} \tag{9}$$

and the  $P$ -wave velocity in the horizontal direction is:

$$V_{ph} = \sqrt{\frac{C_{22}}{\rho}},$$

where

$$C_{22} = \frac{E_2(E_2 - E_1 \nu_{21}^2)}{(1 + \nu_{32})(E_2 - 2E_1 \nu_{21}^2 - E_2 \nu_{32})} \tag{10}$$

The  $S$ -wave velocity in the vertical direction on the plane 1-2 (or plane 1-3) is:

$$V_s = \sqrt{\frac{C_{44}}{\rho}}, \text{ where } C_{44} = G_{12} \tag{11}$$

Two more equations are needed to obtain five unique constants, and we used consolidation test data to obtain them. During the consolidation test on triaxial specimen, incremental hydrostatic stresses ( $\Delta\sigma_1 = \Delta\sigma_2 = \Delta\sigma_3$ ) were applied. Because of the transversely isotropic condition

( $\Delta\varepsilon_2 = \Delta\varepsilon_3$ ) in triaxial specimens, the increment in volumetric strain  $\Delta\varepsilon_v$  can be expressed as:

$$\Delta\varepsilon_v = \Delta\varepsilon_1 + 2\Delta\varepsilon_2 \tag{12}$$

And from Eq. (5),

$$\Delta\varepsilon_1 = \frac{\Delta\sigma_1}{E_1} - \frac{\nu_{21}}{E_2} \Delta\sigma_2 - \frac{\nu_{21}}{E_2} \Delta\sigma_3 \tag{13}$$

$$\begin{aligned} \Delta\varepsilon_2 &= -\frac{\nu_{21}}{E_2} \Delta\sigma_1 + \frac{\Delta\sigma_2}{E_2} - \frac{\nu_{23}}{E_2} \Delta\sigma_3 \\ &= (\Delta\varepsilon_v - \Delta\varepsilon_1) / 2 \end{aligned} \tag{14}$$

In which  $\Delta\varepsilon_v$  and  $\Delta\varepsilon_1$  were measured from the consolidation test due to small changes in principal stresses ( $\Delta\sigma_1, \Delta\sigma_2, \Delta\sigma_3$ ). Figures 3 and 4 show volumetric strain and vertical strain measurements, respectively, during the consolidation process for AP, MT, and MV specimens.

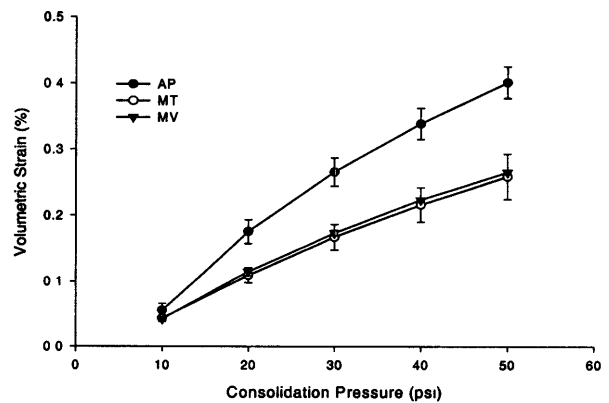


Fig. 3. Volumetric strain against consolidation pressure for AP, MT, and MV specimens (1 psi = 6.89 kPa)

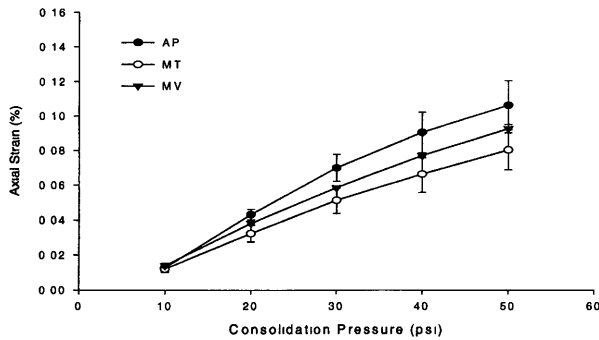


Fig. 4. Axial strain against consolidation pressure for AP, MT and MV specimens (1 psi = 6.89 kPa)

Table 3. Computed elastic moduli from laboratory experiments

Specimens	$E_1$ (MPa)	$E_2$ (MPa)	$G_{12}$ (MPa)	$E_1/E_2$
Air Pluviation (AP)	238	196	73	1.21
Moist Tamping (MT)	242	234	104	1.03
Moist Vibration (MV)	270	261	113	1.03

Tangent moduli (slope of the curves) at 68.9 kPa (10 psi) consolidation stress on the curves in Figs. 3 and 4 were used to calculate  $\Delta\varepsilon_v$ , and  $\Delta\varepsilon_1$  during this analysis, respectively. The application of consolidation test data to Eqs. (13) and (14) to obtain the elastic constants is justified, since the incremental stress-strain relation is in an elastic range although the entire consolidation process involves a large strain (non-elastic) behavior.

$G_{12}$  is solved directly from Eq. (11). The remaining elastic constants ( $E_1, E_2, G_{23}, \nu_{12}, \nu_{21}, \nu_{23}, \nu_{32}$ ) were solved by using Eqs. (6), (7), (8), (9), (10), (13), and (14). Since these equations are non-linear, a commercial computer program, Mathematica, was used to solve the problem.

**RESULTS AND DISCUSSIONS**

*Cyclic Stress Ratio to Cause Liquefaction*

Volumetric and vertical strain data under isotropic stress conditions (Figs. 3 and 4) clearly show that the preparation techniques caused significant differences in those behaviours. It was observed that the amount of volumetric strain ( $\varepsilon_v$ ), and the axial strain ( $\varepsilon_1$ ) were the highest for AP specimens, followed by MV, and MT specimens in the order. It suggests that AP specimens had the lowest stiffness and the highest tendency for volume changes and thus potentially lowest resistance against liquefaction. Figure 5 shows cyclic stress ratios to cause liquefaction for three differently prepared samples in the laboratory. AP (air pluviation) specimens exhibited the weakest liquefaction resistance while MV (moist vibration) showed the strongest resistance. The MT (moist tamping) specimen was slightly weaker than MV, but much stronger than AP. Figure 6 shows the DEM simulated liquefaction resistant (Ishibashi and Kiku, 1995) applying constant cyclic simple shear strain  $\gamma_{cyclic}$  on

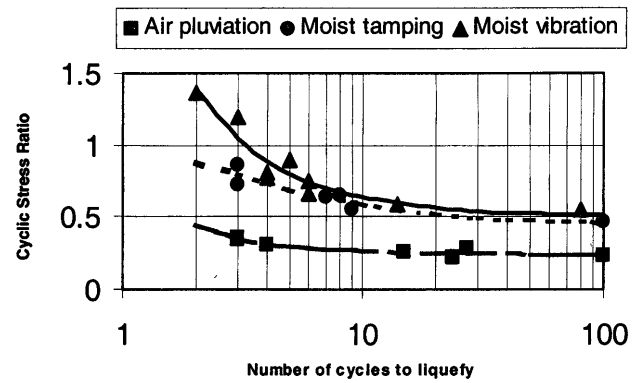


Fig. 5. Laboratory liquefaction test results for medium loose ( $D_r = 50\%$ ) Virginia Beach Sand

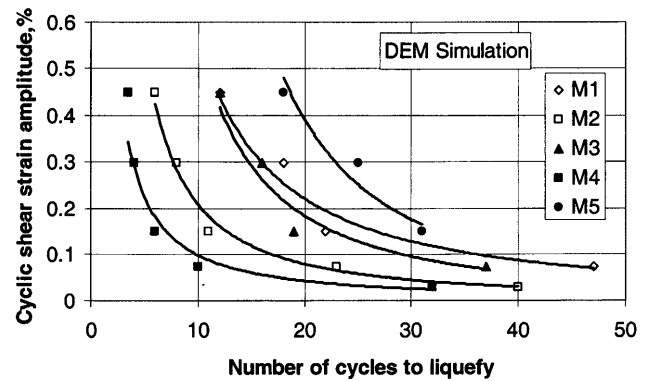


Fig. 6. DEM simulated liquefaction test results under constant cyclic shear stress application

the vertical-horizontal plane. In the simulations, the initial liquefaction was defined as a condition at which the equivalent pore water pressure ratio reached 0.9 level (1.0 ratio as complete liquefaction), beyond that the equivalent pore water pressure vs.  $N$  curve showed clear flows under constant cyclic shear strain application. The M5 specimen was strongest and was followed by M1, M3, M2, and M4 in that order. Note that the M1 specimen was purely isotropic. In the early DEM simulation study, after trials and errors, we found that the moduli parameter  $G_{average}/(E_1/E_2)^3$  was a unique quantity to bring liquefaction resistance curves to a unified curve, where  $E_1$  and  $E_2$  are compression moduli in the vertical ( $\theta=0^\circ$ ) direction, and in the horizontal ( $\theta=90^\circ$ ) direction, respectively, and  $G_{average}$  is the average shear modulus from different directions ( $\theta=0^\circ, 15^\circ, 30^\circ, 45^\circ, 60^\circ, 75^\circ, 90^\circ$ ) of shear distortion. Accordingly, Fig. 6 was replotted in Fig. 7 with a modified vertical axis  $\gamma_{cyclic}/G_{average}/(E_1/E_2)^3$  in %/MPa unit. All the curves in Fig. 6 converged into a narrowly banded zone as seen in Fig. 7. Next, the laboratory cyclic stress ratio curves (Fig. 5) were divided by the same moduli parameter,  $G_{average}/(E_1/E_2)^3$  in Fig. 8. In the figure,  $G_{12}$ , instead of  $G_{average}$ , was used since the change of  $G$  values with the directional shear distortion was not significant, as will be observed in the following section. Indeed three curves in Fig. 5 converged to a unique curve in Fig. 8 by this procedure.

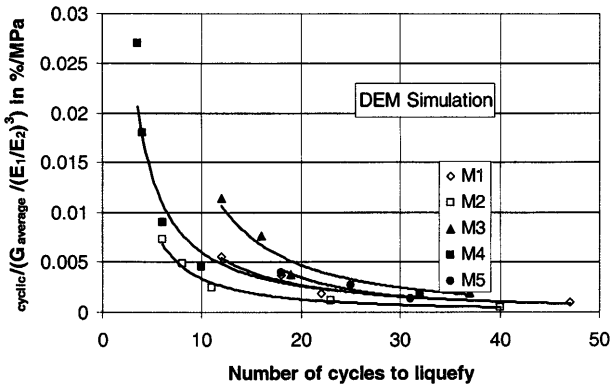


Fig. 7. DEM simulated liquefaction test data divided by  $G_{average}/(E_1/E_2)^3$

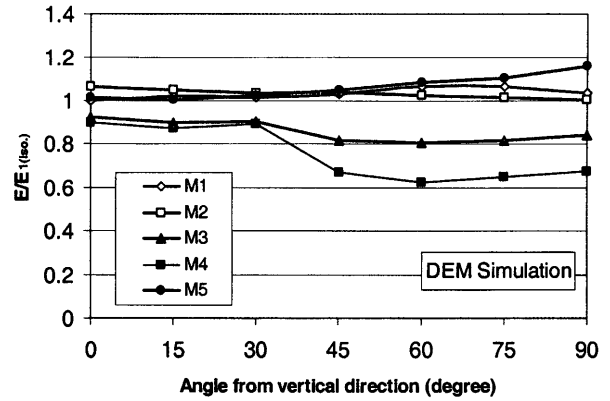


Fig. 9. Change of  $E$  values with various directions of compression—DEM simulation

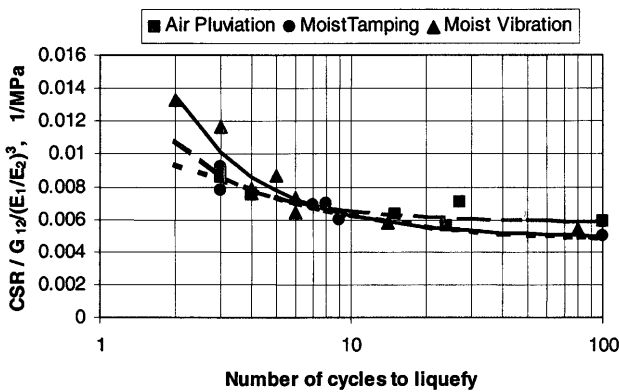


Fig. 8. Laboratory liquefaction test data divided by  $G_{12}/(E_1/E_2)^3$

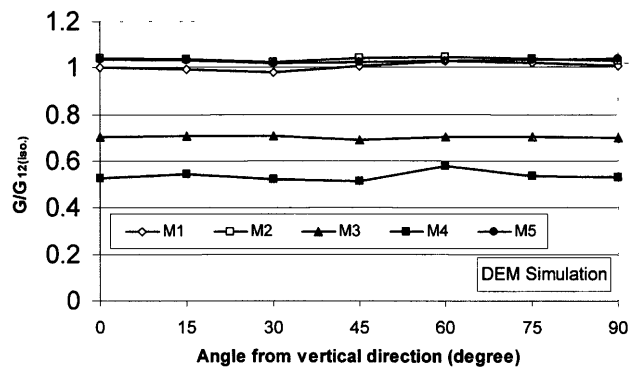


Fig. 10. Change of  $G$  values with various directions of shear distortion—DEM simulation

*Transversely Isotropic Elastic Constants and Relations to Anisotropy*

Earlier DEM simulations gave the variations of directional  $E$  and  $G$  as seen in Figs. 9 and 10, respectively. As seen in Fig. 9, longitudinal moduli  $E$  varied significantly with the  $\theta$  angle for the M3 and M4 specimens, while the moduli did not change much for the M1, M2 and M5 specimens. The former group is considered highly anisotropic in comparison with the latter group of specimens. On the other hand, Fig. 10 shows that there were no significant variations of the  $G$  value with the change of  $\theta$  angle for all specimens. However, the whole  $G$  values decreased when the level of anisotropy increased as seen that the M3 and M4 specimens showed considerably lower  $G$  values relative to  $G_{12(iso)}$  ( $G$  value of isotropic specimen). From these two figures it can be said that when the level of anisotropy increases  $E$  decreases from the vertical direction to the horizontal direction (that is,  $E_1/E_2$  increases), and  $G$  decreases regardless of the directions.

Computed  $E_1$ ,  $E_2$  and  $G_{12}$  values based on the laboratory measurements are summarized in Table 3 for confining pressure of 68.9 kPa. From the MV specimen to the AP specimen,  $E_1$  shows the smallest reduction (12%),  $E_2$  shows slightly larger drop (25%), and  $G_{12}$  shows the largest drop (35%). The ratio of  $E_1/E_2$  for MV and MT

are nearly the unity (1.03), while the ratio for AP is 1.21. That implies that the MV and MT specimens are nearly isotropic and the AP specimen is highly anisotropic. However, the MT specimen's  $G_{12}$  value is slightly (8%) lower than that of the MV specimen, and therefore, it can be said that the MT material is in between the MV and AP materials, but rather close to the MV material.

Based on the above observations on the DEM simulation as well as on laboratory results, the  $E_1/E_2$  ratio is used as an anisotropic index. Figures 11, 12, 13 plot, in log-log scale, normalized  $E_1$ ,  $E_2$ , and  $G_{12}$  values with their isotropic values (i.e.,  $E_1/E_{1(iso)}$ ,  $E_2/E_{2(iso)}$ , and  $G_{12}/G_{12(iso)}$ ) as a function of the anisotropic index  $E_1/E_2$ , respectively. In the figures, for those laboratory data (AM, MT, and MV), the MV specimen is assumed to be isotropic in order to normalize the moduli. Reduction in  $G_{12}/G_{12(iso)}$ , with increase of  $E_1/E_2$ , is the highest followed by  $E_2/E_{2(iso)}$  and  $E_1/E_{1(iso)}$ . That implies that  $G_{12}$  is the most sensitive parameter to anisotropy while  $E_1$  is the least sensitive parameter. Ratios,  $E_1/E_{1(iso)}$ ,  $E_2/E_{2(iso)}$ , and  $G_{12}/G_{12(iso)}$  decrease linearly with increasing  $E_1/E_2$  in log-log scale and the following relations are obtained:

$$\frac{E_1}{E_{1(iso)}} = \left(\frac{E_1}{E_2}\right)^{-0.417} \tag{15}$$

$$\frac{E_2}{E_{2(iso)}} = \left(\frac{E_1}{E_2}\right)^{-1.425} \tag{16}$$



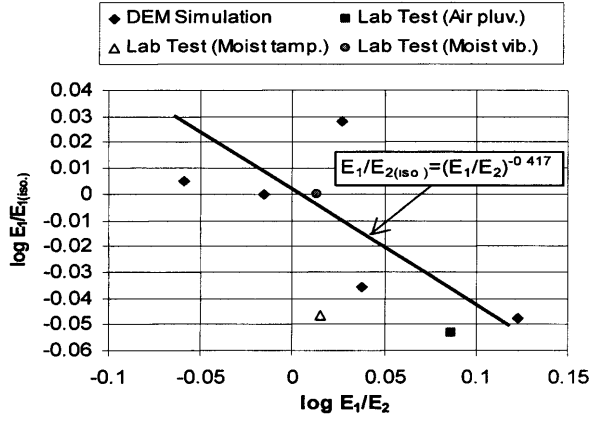


Fig. 11. Relationships between  $\log E_1/E_{1(iso.)}$  and  $\log E_1/E_2$

$$\frac{G_{12}}{G_{12(iso.)}} = \left(\frac{E_1}{E_2}\right)^{-1.985} \quad (17)$$

By using Eqs. (15), (16), and (17) and relations,  $G_{12} = \rho V_s^2$  and  $G_{12(iso.)} = \rho V_{s(iso.)}^2$ , the parameter  $G_{12}/(E_1/E_2)^3$ , which has been used to modify liquefaction resistance curves for DEM and laboratory liquefaction data, can be expressed as:

$$\begin{aligned} \frac{G_{12}}{\left(\frac{E_1}{E_2}\right)^3} &= \left(\frac{E_1}{E_2}\right)^{-5.0} \cdot \frac{G_{12(iso.)}}{\left(\frac{E_{1(iso.)}}{E_{2(iso.)}}\right)^3} = \left(\frac{E_1}{E_2}\right)^{-5.0} \cdot G_{12(iso.)} \\ &= \left(\frac{G_{12}}{G_{12(iso.)}}\right)^{-5.0/(-1.985)} \cdot G_{12(iso.)} \\ &= \left(\frac{\rho V_s^2}{\rho V_{s(iso.)}^2}\right)^{-5.0/(-1.985)} \cdot G_{12(iso.)} \\ &= \left(\frac{V_s}{V_{s(iso.)}}\right)^{5.0} \cdot G_{12(iso.)} = V_s^{5.0} \cdot V_{s(iso.)}^{-5.0} \cdot G_{12(iso.)} \end{aligned} \quad (18)$$

where  $E_{1(iso.)}$  is equal to  $E_{2(iso.)}$  for isotropic materials. Since  $V_{s(iso.)}$  and  $G_{12(iso.)}$  are certain isotropic values for a given soil and density, the above moduli parameter is proportional to 5.0 power of shear wave velocity ( $V_s^{5.0}$ ). Note that Eq. (18) utilized Eqs. (15), (16), and (17) and the computed power of  $V_s$  was 5.045. The relation in Eq. (18) can also be obtained only from Eq. (17). In such case, the power of  $V_s$  was computed as 4.985. Since those equations are from experimental data seen in Figs. 11, 12, and 13, the 5.0 power of  $V_s$  is considered to be reasonable. Figure 14 re-plots laboratory cyclic stress ratio (Fig. 5) divided by  $V_s^{5.0}$ . If Fig. 14 is compared with Fig. 8, Fig. 14 shows similar or even better converged curves than Fig. 8.

**Modified Liquefaction Cyclic Stress Ratio**

Based on the uniqueness of the parameter  $G_{12}/(E_1/E_2)^3$  on liquefaction resistance, modified liquefaction cyclic stress ratio can be expressed as:

$$\frac{CSR_N}{\left(\frac{E_1}{E_2}\right)^3} = A \quad (19)$$

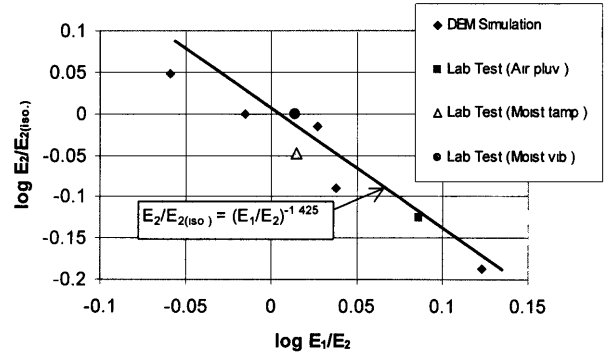


Fig. 12. Relationships between  $\log E_2/E_{2(iso.)}$  and  $\log E_1/E_2$

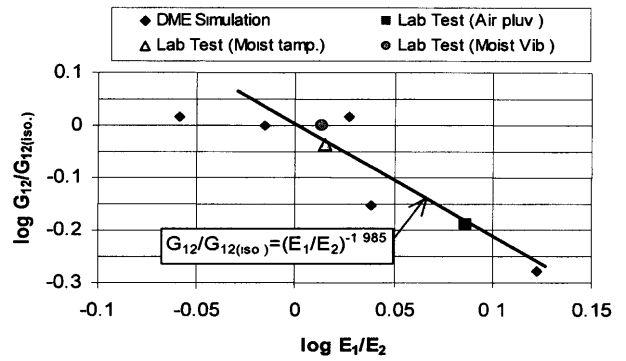


Fig. 13. Relationships between  $\log G_{12}/G_{12(iso.)}$  and  $\log E_1/E_2$

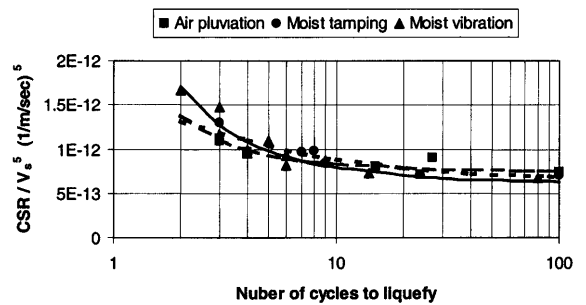


Fig. 14. Laboratory liquefaction cyclic stress ratio divided by  $V_s^{5.0}$

Constant A is only a function of soil type and density and is not influenced by the level of anisotropy like those created by different sample preparation techniques. Therefore, using Eqs. (18) and (19) the cyclic stress ratio to cause liquefaction at  $N$  cycles ( $CSR_N$ ) can be written as:

$$CSR_N = A \cdot \frac{G_{12}}{\left(\frac{E_1}{E_2}\right)^3} = A \cdot \left(\frac{V_s}{V_{s(iso.)}}\right)^{5.0} \cdot G_{12(iso.)} \quad (20)$$

Again Eq. (20) shows that  $CSR_N$  is proportional to  $V_s^{5.0}$ .

Next, we define Liquefaction Stress Ratio Reduction Factor (LSRRF) as  $CSR/CSR_{iso.}$ , which is the ratio of liquefaction cyclic stress ratio of any anisotropic soil to that of isotropic soil with the same density.

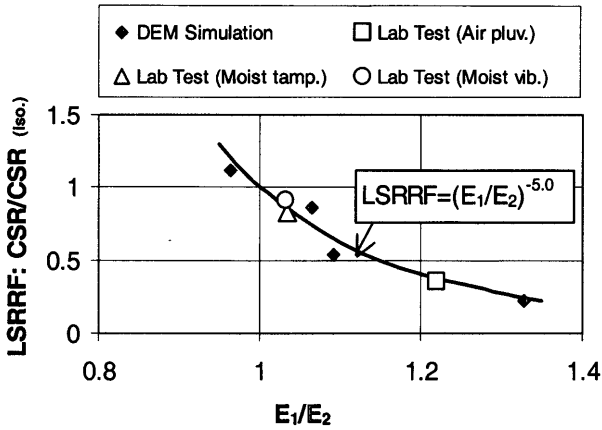


Fig. 15. Liquefaction stress ratio reduction factor vs.  $E_1/E_2$

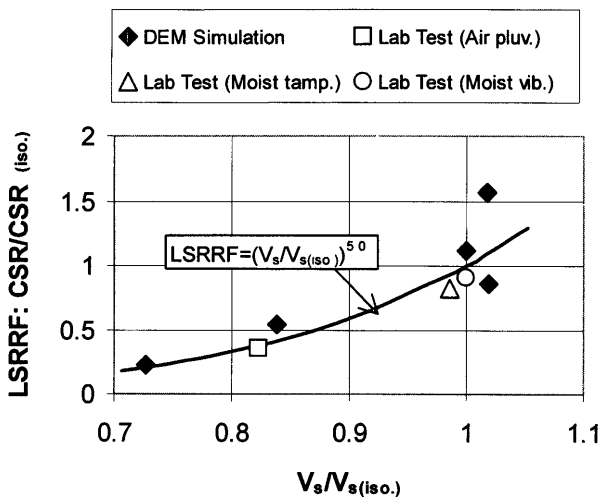


Fig. 16. Liquefaction stress ratio reduction factor vs.  $V_s/V_{s(ISO)}$

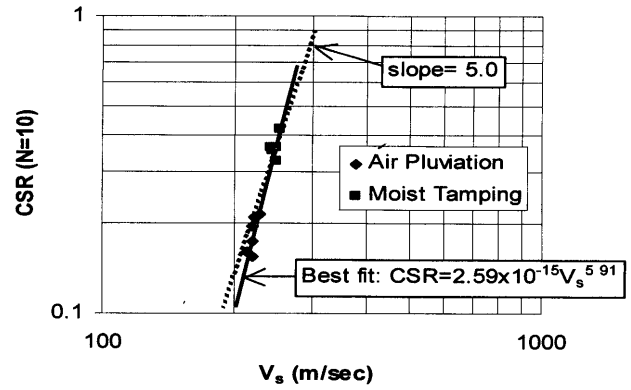


Fig. 17. Cyclic stress ratio vs.  $V_s$  based on De Alba et al. data (1984) (Dover 40-50 sand)

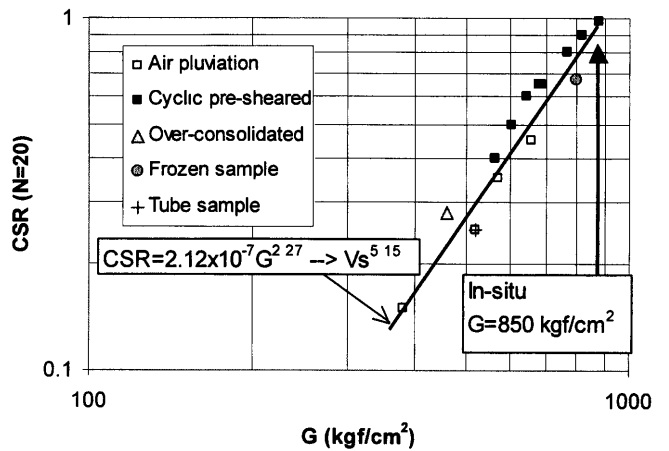


Fig. 18. Cyclic stress ratio vs. shear modulus  $G$  based on Tokimatsu et al. data (1986) (Niigata sand) ( $1 \text{ kgf/cm}^2 = 98.1 \text{ kPa}$ )

$$LSRRF = CSR/CSR_{iso.}$$

$$= \left( A \cdot \frac{G_{12}}{\left(\frac{E_1}{E_2}\right)^3} \right) / \left( A \cdot \frac{G_{12(ISO.)}}{\left(\frac{E_{1(ISO.)}}{E_{2(ISO.)}}\right)^3} \right)$$

$$= \left(\frac{E_1}{E_2}\right)^{-3.0} \cdot \frac{G_{12}}{G_{12(ISO.)}}$$

$$= \left(\frac{E_1}{E_2}\right)^{-3.0} \cdot \left(\frac{E_1}{E_2}\right)^{-1.985}$$

$$= \left(\frac{E_1}{E_2}\right)^{-5.0}$$

or

$$= \left( A \cdot \left(\frac{V_s}{V_{s(ISO.)}}\right)^{5.0} \cdot G_{12(ISO.)} \right) / \left( A \cdot \left(\frac{V_{s(ISO.)}}{V_{s(ISO.)}}\right)^{5.0} \cdot G_{12(ISO.)} \right)$$

$$= \left(\frac{V_s}{V_{s(ISO.)}}\right)^{5.0} \tag{21}$$

Figures 15 and 16 plot the above equations with  $E_1/E_2$  and  $V_s/V_{s(ISO.)}$ , respectively, alongside DEM and laboratory data. For laboratory liquefaction data, we assume

again that the MV specimen is isotropic material. In another words, for a given soil with a given density, isotropic material has generally the highest liquefaction resistance. Reduction of the liquefaction resistance from an isotropic material to an anisotropic material can be estimated using LSRRF as defined in Eq. (21), or in Figs. 15 and 16 as a function of  $E_1/E_2$  or  $V_s/V_{s(ISO.)}$ .

*Comparisons with Previous Research Work*

Findings of this research are compared with previous researchers' results. In Arulmoli et al.'s (1985) research on Monterey "0" sand, dry pluviated specimen showed a higher anisotropic index value and a lowest liquefaction resistance in comparison with wet pluviated and moist tamped specimens. This is the same result from this research. De Alba et al. (1984) performed liquefaction test with shear wave velocity measurements on Dover 40-50 sand prepared by two different techniques (air pluviation and moist tamping). Figure 17 shows the results in which the best fit curve correlates CSR with  $V_s^{5.91}$ . The slope with 5.0 (value obtained from this research) is also seen in the figure for a comparison. Tokimatsu et al. (1986) also performed similar tests for Niigata sand. The result is seen in Fig. 18, where  $V_s^{5.15}$  was

obtained as the best fitted curve. In the figure it is interesting to see that in-situ measured shear modulus ( $G = 850 \text{ kgf/cm}^2$ ) is located at the nearly highest CSR value. The frozen specimen has nearly the highest value of shear modulus, but still slightly lower than in-situ value. Resistance for the tube-specimen is much smaller than the in-situ value. Air pluviated specimens occupy a lower section of the plot, as we also found from this research. The above observation suggests that field liquefaction resistance is much higher than the one obtained from laboratory AP specimen. The field value may be rather close to the one from MV specimen, which is considered to be rather isotropic. Liquefaction cyclic stress ratio of the AP specimen is about 40% of the MV specimen during this research. Therefore, if the AP specimen will be used for field liquefaction evaluation, it will be an approach that is too conservative. It shall be noted, however, that the above hypothesis may or may not be true for other sites or other types of soil. Further research on validating this will be needed.

## SUMMARY AND CONCLUSIONS

The research was conducted to evaluate anisotropic characteristics of a medium density sand prepared by three different techniques (air pluviation (AP), moist tamping (MT), and moist vibration (MV)). Cyclic stress ratios that cause liquefaction were determined from cyclic triaxial tests. On the same triaxial specimens,  $P$ -wave velocities in the vertical and horizontal directions and one  $S$ -wave velocity on the vertical-horizontal plane were measured using piezoelectric bender elements. With those wave measurements and consolidation test data, transversely isotropic elastic constants were determined. Earlier study (Ishibashi and Kiku, 1995) with discrete element method (DEM) simulations on a granular assembly was incorporated into this research. DEM simulation included liquefaction simulation and directional elastic moduli for five differently prepared specimens. The following conclusions can be drawn from this research.

1. Three differently prepared laboratory specimens showed quite different liquefaction resistances. The MV specimen showed the highest resistance, while the AP specimen shows the weakest. The MT specimen's resistance was rather close to, but slightly less than, that of the MV specimen.
2. DEM simulation showed that when the level of anisotropy increases  $E_1/E_2$  ratio increases and the  $G$  value decreases in all directions. Directional  $G$  values, however, remain nearly constant in all the direction of shear distortion even with changing the level of anisotropy.
3. Elastic constants computed based on the laboratory data indicated that the MV specimen is nearly isotropic while the AP specimen is highly anisotropic. The MT specimen is rather close to the MV specimen, but slightly more anisotropic.
4. It was found from laboratory tests as well as DEM simulations that when liquefaction cyclic stress ratio

is divided by  $G_{12}/(E_1/E_2)^3$  or by  $G_{\text{average}}/(E_1/E_2)^3$ , liquefaction resistance curves (CSR vs.  $N$  relations) converge to a unique curve regardless of sample preparation techniques.

5. It was also found that the cyclic stress ratio that causes liquefaction at the  $N$ th cycle,  $\text{CSR}_N$ , is nearly proportional to  $V_s^{5.0}$ ; thus liquefaction resistance can also be divided with  $V_s^{5.0}$  to obtain a unique resistance curve regardless of sample preparation techniques.
6. The Liquefaction Stress Ratio Reduction Factor (LSRRF) was introduced to estimate the reduction of liquefaction cyclic stress ratio of anisotropic specimen from the isotropic specimen as simple functions of  $(E_1/E_2)^{-5.0}$  or  $(V_s/V_{s(\text{iso})})^{5.0}$ .
7. In comparison with previous researchers' findings, field liquefaction resistance may be close to that of the isotropic specimens, which is close to that of the MV specimen. The AP specimen is highly anisotropic and showed very low liquefaction resistance, which is conservative but non-economical when used for design. This hypothesis shall be validated for other sites and other types of soil in the future.

## REFERENCES

- 1) Agarwal, T. K. and Ishibashi, I. (1992): Anisotropic elastic constants of granular assembly from wave velocity measurements, *Advances in Micromechanics of Granular Materials*, (eds. by Shen, H. et al.), Elsevier, 51-60.
- 2) Andrus, R. D. and Stokoe, K. H. (2000): Liquefaction resistance of soils from shear wave velocity, *J. of Geotech. and Geoenvironmental Engrg.*, **126**(11), 1015-1025.
- 3) Arulmoli, K., Arulanandan, K. and Seed, H. B. (1985): New method for evaluation liquefaction potential, *J. of Geotech. Engrg.*, **111**(1), 95-114.
- 4) Capar, O. F. (2000): *Determination of Anisotropy of Granular Materials and Its Relation to Liquefaction Resistance under Cyclic Loading*, Ph.D. dissertation, Old Dominion University, Norfolk, Virginia.
- 5) Cundall, P. A. (1988): Computer simulations of dense sphere assemblies, *Mechanics of Granular Materials*, (eds. by Satake, M. and Jenkins, J. T.), Elsevier, 113-123.
- 6) De Alba, P., Baldwin, K., Janoo, V., Roe, G. and Celikkol, B. (1984): Elastic-wave velocities and liquefaction potential, *Geotech. Testing J.*, **7**(2), 77-87.
- 7) Dyvik, R. and Madhus, C. (1985): Lab measurements of  $G_{\text{max}}$  using bender elements, *Proc. of Recent Advances in Instrumentation, Data Acquisition and Testing in Soil Dynamics*, ASCE, 79-107.
- 8) Finn, W. D. L., Vaid, Y. P. and Bhatia, S. K. (1978): Constant volume cyclic simple shear testing, *Proc. 2nd Int. Conf. on Microzonation*, San Francisco, 2, 839-851.
- 9) Ishibashi, I. and Agarwal, T. K. (1991): Multi-directional wave velocity by piezoelectric crystals, *Proc. of Recent Advances in Instrumentation Data Acquisition and Testing in Soil Dynamics*, ASCE, 102-117.
- 10) Ishibashi, I. and Kiku, H. (1995): Effect of initial anisotropy on liquefaction potential by discrete element model., *Proc. First Int. Conf. on Earthquake Geotech. Engrg. (IS-TOKYO '95)*, (ed. by Ishihara, K.), II, Balkema, Rotterdam, 863-868.
- 11) Ladd, R. S. (1974): Specimen preparation and liquefaction of sands, *J. of Geotech. Engrg. Div.*, **100**(GT10), 1180-1184.
- 12) Muliilis, J. P., Seed, H. B., Chan, C. K., Mitchell, J. K. and Arulanandan, K. (1977): Effects of sample preparation on sand liquefaction, *J. of the Geotech. Engrg. Div.*, **103** (GT, GT2), 91-108.

- 13) Tatsuoka, F., Ochi, K., Fuji, S. and Okamoto, M. (1986): Cyclic undrained triaxial and torsional shear strength of sands for different sample preparation methods, *Soils and Foundations*, **26** (3), 23-41.
- 14) Thomann, T. G. and Hryciw, R. D. (1990): Laboratory measurement of small strain modulus under  $k_0$  conditions, *Geotech. Testing J.*, **13**(2), 97-105.
- 15) Toki, S., Tatsuoka, F., Miura, S., Yoshimi, Y., Yasuda, S. and Makihara, Y. (1986): Cyclic undrained triaxial strength of sand by a cooperative test program, *Soils and Foundations*, **26**(3), 117-138.
- 16) Tokimatsu, K., Yamazaki, T. and Yoshimi, Y. (1986): Soil liquefaction evaluations by elastic shear moduli. *Soils and Foundations*, **26**(1), 25-35.
- 17) Tokimatsu, K. and Uchida, A. (1990): Correlation between liquefaction resistance and shear wave velocity, *Soils and Foundations*, **30**(2), 33-42.
- 18) Yoshimi, Y., Tokimatsu, K., Kaneko, O. and Makihara, Y. (1984): Undrained cyclic shear strength of a Niigata sand, *Soil and Foundation*, **24**(4), 131-145.
- 19) Yoshimi, Y., Tokimatsu, K. and Hosaka, Y. (1989): Evaluation of liquefaction resistance of clean sands based on high-quality undisturbed samples, *Soils and Foundations*, **29**(1), 93-104.